ELECTRON CYCLOTRON HEATED LOW TO HIGH MODE TRANSITION IN KSTAR

H. JHANG, M. J. CHOI, H. RIZVI, H. S. KIM Korea Institute of Fusion Energy 169-148 Gwahak-ro, Yuseong-gu, Daejeon, 34133, Republic of Korea Email: hgjhang@kfe.re.kr

Abstract

This study investigates the experimental characteristics of the Low-to-High (L-H) transition induced by Electron Cyclotron Resonance Heating (ECRH) in KSTAR. A pre-transition density scan reveals a characteristic minimum density required for the transition. This minimum density in KSTAR is found to be lower than the value predicted by a scaling law proposed by Ryter et al. [Nucl. Fusion 54, 083003 (2014)]. Using Electron Cyclotron Emission Imaging (ECEI) diagnostics, a comprehensive analysis of low-wavenumber electron temperature fluctuations was conducted. As the transition fully develops, a coherent mode emerges, chirping down from ~60 to ~20 kHz. This mode is shown to revive turbulence that had been significantly suppressed during the initial LH transition phase. The revived turbulence could be a possible explanation for the absence of large Edge Localized Modes (ELMs) when the coherent mode persists in ECRH-induced H-mode plasmas. Finally, we explore the theoretical possibility that the coherent mode could be an edge-localized Alfvén wave.

1. INTRODUCTION

Electron cyclotron resonance heating (ECRH) is a reliable heating source in the contemporary and future magnetic fusion devices. In fact, ECRH is supposed to be the dominant heating method in the initial operation of some planned devices, such as ITER and Divertor Tokamak Test facility (DTT), and ST-40. Achieving an H-mode in the early stage of operation with a low field and a low plasma current is necessary to assure the integrity of the device and the efficacy of edge localized mode (ELM) control tools such as resonant magnetic perturbation coils. This is essential for accomplishing the subsequent scientific goal of the ITER mission with full machine capability. In this regard, there has been a rekindled interest in the study of ECRH dominant LH transitions in terms of both the macroscopic phenomenology and a detailed study of micro-turbulence evolution. The successful LH transition using only ECRH has been demonstrated in many tokamak experiments [1-3]. This result, in fact, has been reckoned as evidence of the possibility to access H-mode with different heating methods. In particular, a recent AUG experiment demonstrates that the H-mode sustained by ECRH could be operated in a stationary ELM-free state [4]. This operation regime is pertinent to the enhanced D-alpha (EDA) H-mode developed on Alcator C-Mod that is characterized by dominant electron heating, low momentum input, and high density. The ELM-free state in AUG, similar to Alcator C-Mod, is shown to be correlated with the appearance of the quasi-coherent mode (QCM) emerging during the LH transition. The physical mechanism responsible for triggering QCM and its role in pedestal transport are to be evaluated further. The objective of this work is to study the experimental characteristics of the ECRH-produced LH transition in KSTAR plasmas. Specifically, we examine features of the LH transition and the H-mode state driven and sustained by ECRH. The evolution of microscopic fluctuations before, during, and after the transition is also scrutinized. Further, we explore the physics of the coherent mode which appears during the LH transition and prevails for the H-mode state. The possibility of edge-localized Alfvén eigenmodes (ELAEs) is discussed, focusing on how they may arise from the change in magnetic shear induced by the bootstrap current inside the edge pedestal.

2. EXPERIMENTAL SET-UP AND MINIMUM DENSITY

To study characteristics of the ECRH-driven H-mode, we use two second harmonic X-mode ECRH systems in KSTAR. The injection power for the first and the second ECRH systems is 0.7 and 0.68MW, respectively, comprising a total power of 1.38 (MW). Typical discharge parameters in these experiments are as follows: the magnetic field at the geometric center $B_T = 1.8$ (T), the plasma current $I_p = 0.6$ (MA), the safety factor at the 95% flux surface is $q_{95} = 4.2$, and the working gas is deuterium. The plasma shape is lower single null with favorable magnetic configuration in terms of LH transition. In this power level and experimental conditions, the KSTAR plasma makes an LH transition depending on the value of pretransition L-mode density (<n>pre). In this series of experiments, we scan the L-mode pre-transition density while fixing ECH power maximum available at KSTAR. For some shots, we tried to inject supersonic molecular beam injection (SMBI) as an effort to reduce the power threshold.

Figures Figures 1(a)–1(d) show time traces of plasma parameters during a reference discharge exhibiting LH transition with only ECRH. The pre-transition density is $2.0 \times 10^{19} \,\mathrm{m}^{-3}$ in this shot. Density control, which is active up to t=6 sec in this discharge, prevents the ECRH-induced density pump-out from occurring before the LH

transition, hence maintaining pre-transition density. The line-averaged density drifts down a little after density control off and jumps after \sim 500ms of dwell time before initiation of the LH transition. Figures 1(c) and 1(d) show the density (n_e) and electron temperature (T_e) profiles in terms of the normalized minor radius (r/a) at three different time points: t=5.0 s with P_{ECRH}=0.7 (MW) (red), t=5.0 s with P_{ECRH}=0.7 (MW) (blue, L-mode), and t=5.0 s with P_{ECRH}=0.7 (MW) (black, H-mode). The n_e and T_e profiles are measured by a reflectometer and ECE, respectively. The yellow shaded region in Fig. 1(d) denotes the outermost radial position where ECEI measurements of T_e fluctuations are taken. One can see the development of a density p edestal at the H-mode phase. The core electron temperature increases after the second ECRH application and then initially rises further as the LH transition initiates. However, it drops as the density pedestal builds up. In spite of the core T_e drop, a relatively wide T_e pedestal develops in the edge region [Fig. 1(d)].

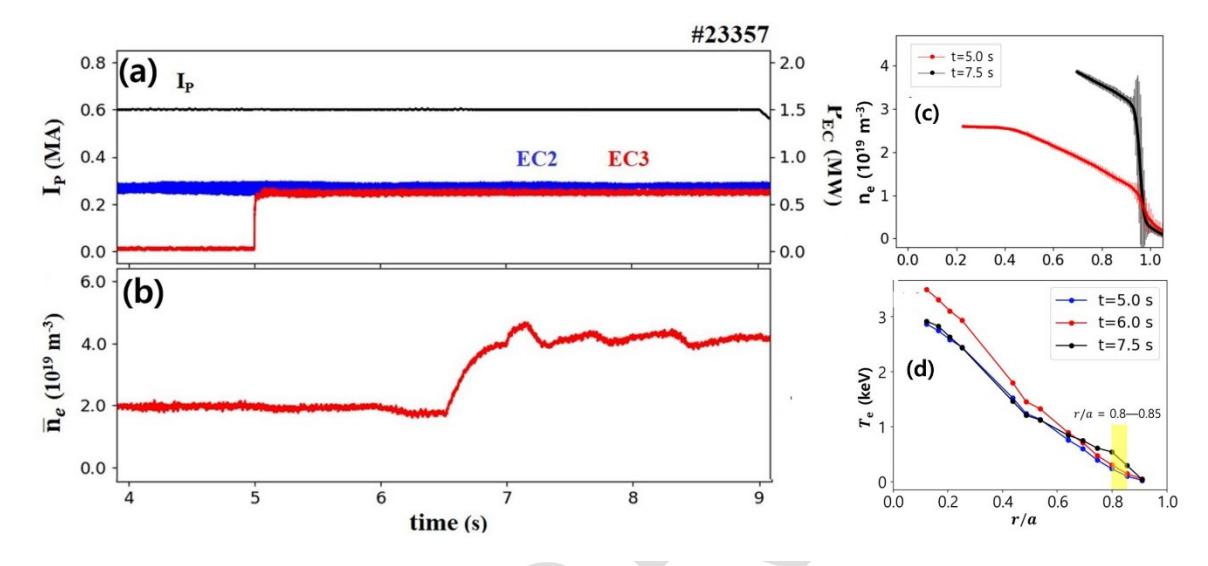


FIG. 1. Time evolutions of (a) plasma current (I_P , black), the first (blue) and the second ECRH power (red), (b) line-averaged density measured by two color interferometry (TCI) during KSTAR discharge #23357 exhibiting LH transition with only ECRH. (c) Density and (d) electron temperature profiles in terms of normalized minor radius [r/a] at different time points: $t=5.0 \, s$ with $P_{ECRH}=0.7 \, MW$ (red), $t=6.0 \, s$ with $P_{ECRH}=1.38 \, MW$ (blue, L-mode), and $t=7.5 \, s$ with $P_{ECRH}=1.38 \, MW$ (black, H-mode). Shaded region in (d) represents the outermost radial position where ECEI measurements are taken. [H Jhang et al, Phys. Plasmas, 31, 092501; licensed under a Creative Commons Attribution (CC BY) license]

Then, one expects the appearance of a density window within which the LH transition happens, owing to the existence of the characteristic U-shaped P_{LH} curve in terms of density. It is of interest to study if the minimum density value obtained in KSTAR experiments is consistent with an empirical scaling law proposed in Ref. [5] based on electron-ion collisional heat exchange. Indeed, results recuperates the characteristic U-shape curve in transition power (P_{LH}) vs. density, exhibiting minimum density for LH transition. From the analysis of data from density scan, we found that the the minimum density in KSTAR (i.e., minimum density in the P_{LH} vs. density curve) is in the range $1.86 < n_{min} < 2.0 \times 10^{19}$ m⁻³. This is $\sim 30\%$ smaller than n_{min} estimated from the scaling law in Ref. [5] whose value is $n_{min} = 2.73 \times 10^{19}$ m⁻³. The tendency to deviate from the Ryter scaling toward a lower density is also seen in JT-60U data, as reported in [5]. The source of this downward shift is uncertain. A hypothesis behind this phenomenon is a possible contrast in the pre-transition E_r well structure, which can arise from differences in the pedestal-like pretransition density profile in the L-mode edge. This hypothesis is based on different SOL conditions depending on the device, though it is speculative at the moment.

3. L-MODE EDGE FLUCTUATION CHARACTERISTICS: DISPERSION PLOTS

In this section, we study how the near-edge fluctuations evolve from an L-mode to a well-realized H-mode state in ECR heated plasmas. We use of ECEI diagnostics measuring low-k Te fluctuations for this purpose. The density fluctuation measurement is made available using the Collective Scattering System (CSS), because no neutral beam-based diagnostic measurements are available. A system of KSTAR ECEI diagnostics measures the radial variation of the poloidal wavenumber and the phase velocity of T_c fluctuations. The spatiotemporal resolution of the ECEI system is $k_{\perp}\rho_i$ <0.5 and Δt =2 µsec, respectively. In this section, we use T_c measured at the most outer channel providing reliable data, which is at r/a= 0.85, to study characteristics of fluctuation evolution during the LH transition. We consider three representative cases to investigate possible differences in T_c fluctuation characteristics: (1) the unsuccessful LH transition due to high pre-transition density, (2) the unsuccessful LH

transition due to low ECRH power, and (3) the successful LH transition at $\sim n_{min}$ with full ECRH power.

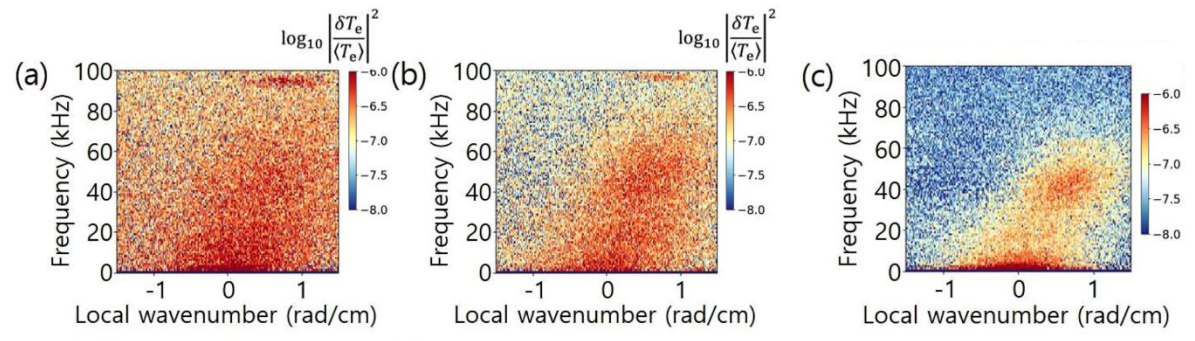


FIG. 2. T_e fluctuations representing frequency (f) vs wavenumber (k) at three different time points corresponding to (a) t=4.8 sec with P_{ECRH} =0. 7 MW, (b) t=5.2 sec with P_{ECRH} =1. 38 MW, and (c) t=7.75 sec with P_{ECRH} =1. 38 MW. Application of the second ECRH intensifies the relative strength of the modes rotating in the electron diamagnetic direction (e-modes) in the laboratory frame. [H Jhang et al, Phys. Plasmas, 31, 092501; licensed under a Creative Commons Attribution (CC BY) license]

We first consider the case where the LH transition is unsuccessful due to high pre-transition density, n_{pre} =3.0×10¹⁹ m⁻³. Figure 2 shows dispersion plots for T_e fluctuations representing frequency (f) vs. local wavenumber (k) at three different time points corresponding to t= 4. 8 sec with P_{ECRH} =0. 7 MW (a), t=5.2 sec with P_{ECRH} =1.38 MW (b), and t=7:75 sec with the same power as (b). The positive (negative) wavenumber means that the mode rotates in the electron (ion) diamagnetic direction in the laboratory frame. We refer to these modes as e- and i-modes, respectively. The application of additional ECRH power intensifies the relative strength of e-modes. The e-mode is persistent during the entire discharge after the second ECRH is applied. Fluctuations exhibit a clear dispersive feature with a positive slope in the dispersion plot, as shown in Figs. 2(b) and 2(c). This implies that the e-modes arise as dominant fluctuations as ECRH power increases. To calculate the average phase velocity of the modes, we employ a statistical method. In this approach, one defines an average phase velocity $< v_p >$ as

$$\langle v_p \rangle = \langle \omega/k_\theta \rangle \equiv \int \hat{S}(k_\theta, \omega)(\omega/k_\theta) d\omega dk_\theta,$$

where $S(k_{\theta},\omega)$ is a normalized spectral power of the ECEI signal. In addition to the phase velocity, we calculate an average group velocity $< v_g >$ considering data from the dispersion plot in the frequency range 20 < f < 100 kHz. From these calculations, we obtain $< v_p > = 4.33$ and $< v_g > = 3.74$ km/sec using the fluctuation data shown in Fig. 2(c). There are no notable changes in fluctuations up to the termination of the discharge in this case—the edge remains in an L-mode with e-modes as dominant fluctuations.

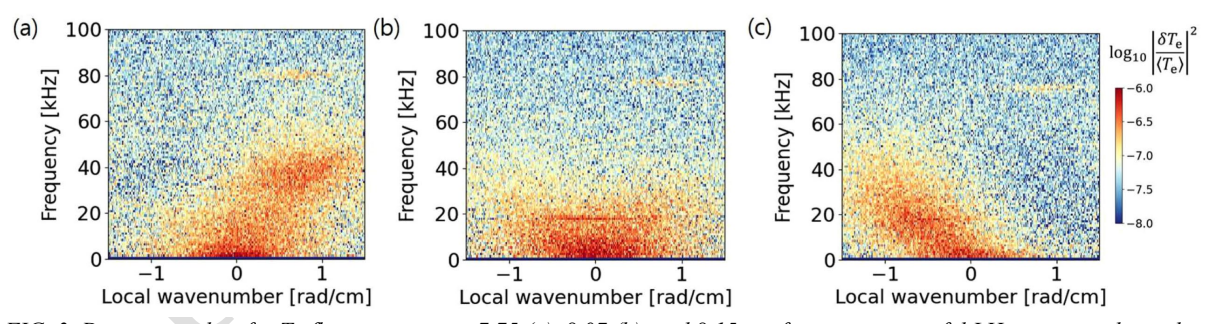


FIG. 3. Dispersion plots for Te fluctuations at t=7.75 (a), 8.07 (b), and 8.15 sec for an unsuccessful LH transition due to low $P_{ECRH}=0.7$ MW. $n_{pre}=2.0\times10^{19}$ m⁻³. Dominant modes flip from electron to ion during a discharge. [H Jhang et al, Phys. Plasmas, 31, 092501; licensed under a Creative Commons Attribution (CC BY) license]

Next, we consider a different case of unsuccessful LH transition due to low power. In this discharge, n_{pre} =2.0×10¹⁹ m⁻³ with P_{ECRH} =0.7 MW. The most interesting observation in this case is that dominant fluctuations flip from eto i-modes during a discharge. This case is in clear contrast to the previous one, where the e-mode remains as the dominant fluctuation during a discharge. Figures 3(a)–3(c) show this phenomenon by presenting dispersion plots at t=7.75, 8.07, and 8.15 sec. The apparent phase and group velocities change their signs from positive to negative ones during a short time period. For instance, $\langle v_p \rangle$ changes from 3.36 km/sec at t=7.75 sec to -2.41 km/sec at t=8.15 sec. The i-mode develops gradually, beginning from a low frequency band, as shown in Fig. 3(b), extending to a higher one, hence completing the dispersion of the mode. The duration of the mode transition period is $\Delta t \sim$ 203 msec. During the mode transition period, T_e changes little before and during the transition period. It begins

to drop after the mode transition is almost completed. From this observation, the density reduction from 2.0×10^{19} m⁻³ at the initial time point of the mode transition will likely be responsible for the fluctuation characteristic change (not shown in the figure). After completion of the mode transition, electron density attains 1.64×10^{19} m⁻³. The computed collisionality during the time window is low (below 1.5), leading to reduced emode fluctuation amplitude. After mode transition, the collisionality increases a little due to decrease in T_e , albeit still weak. At the moment, it is unclear if this mode transition event is an apparent phenomenon due to the change in equilibrium $E \times B$ velocity during the mode transition window or an actual one accompanying the change in dominant instability. To clarify this, we need to evaluate the fluctuation characteristics in the plasma frame, which is unavailable in this work. Of course, the emergence of ion modes is also possible, which requires further detailed study. In spite of the significant change in mode characteristics, however, the relative amplitude of fluctuations is kept almost constant, which is a possible origin of the failure to achieve LH transition in this case.

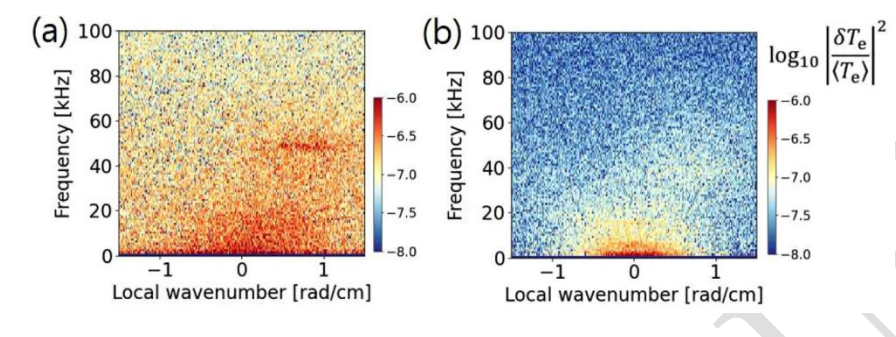


FIG. 4. Dispersion plots for T_e fluctuations when $n_{pre}=2.2\times10^{19}$ m⁻³ at (a) t=4.8 sec with $P_{ECRH}=0.7$ MW and (b) t=7.05 sec with $P_{ECRH}=1.38$ MW. The second ECRH leads to a strong reduction in T_e fluctuations at the high frequency. [H Jhang et al, Phys. Plasmas, 31, 092501; licensed under a Creative Commons Attribution (CC BY) license]

Finally, we consider the case where a successful LH transition happens when n_{pre} =2.2×10¹⁹ m^{-3} and P_{ECRH} =1.38 MW. In this discharge, the LH transition begins to start at t=7.1 sec, which is ~100 msec after deactivation of the density control system. chirping period. Figure 4 shows a clear distinction in T_e fluctuations between this case and cases shown in Fig. 2 where the same amount of power is applied to a higher pre-transition density. In this discharge, the application of the second ECRH results in a strong reduction in T_e fluctuations at the high frequency region, i.e., $f > \sim 15$ kHz. In contrast, modes with high frequencies are clearly seen when $n_{pre} > n_{min}$, as shown in Figs. 2(b) and 2(c). Initially, fluctuations are nearly symmetric in positive and negative wavenumbers, signifying the existence of both e- and i-modes, which is similar to Fig. 3(b). The T_e fluctuations remain in a nearly symmetric pattern even after the second ECRH is applied. The fluctuation frequency is limited within ~ 15 kHz, as shown in Fig. 4(b). This indicates that the amplitudes of higher-frequency fluctuations are significantly reduced when the plasma approaches the LH transition point. The existence of such low-frequency isotropic fluctuations prior to LH transition coincides with the observation of dual modes near the LH transition point at DIII-D [6]. During the LH transition period, the fluctuation amplitude drops in an isotropic fashion, which corroborates the popular paradigm of the E×B shear suppression of low-k fluctuations as an origin for the transport bifurcation.

4. EDGE COHERENT MODE AND TURBULENCE EVOLUTION

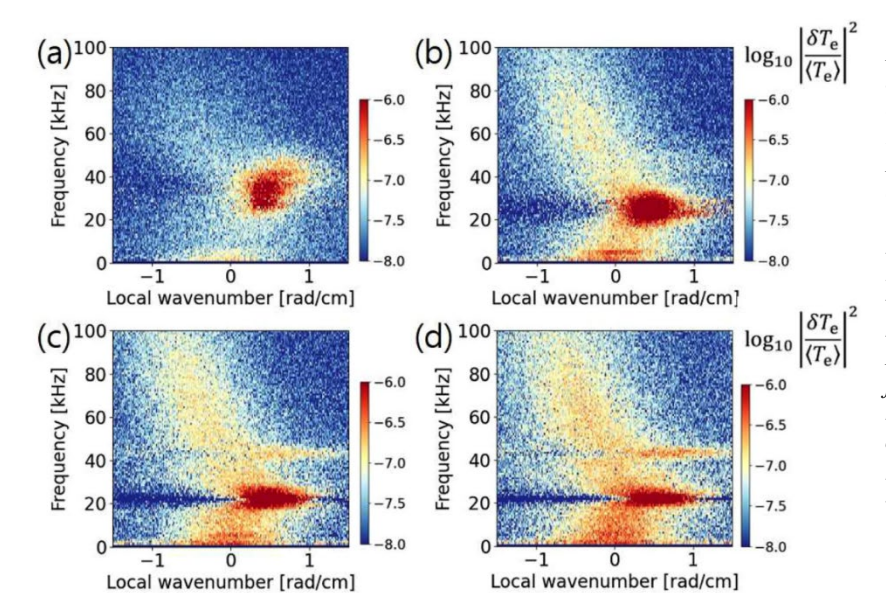


FIG. 6. Dispersion plots during and after the LH transition, exhibiting ECM evolution and recurrence of fluctuations at the H-mode phase. Time points corresponding to (a)-(d) are t=7.25, 7.35, 7.45, and 7.55 sec, respectively. Coherent mode begins to appear at t=7.15 s with f~60 kHz. Low-frequency modes begin to reappear as the strengthens. Higherfrequency ion modes with a negative group velocity also appear during the H-mode state. [H Jhang et al, Phys. Plasmas, 31, 092501; licensed under a Creative Commons Attribution (CC BY) license]

A prominent feature occurring during a successful LH transition near the minimum density (n_{min}) is the emergence of an Edge Coherent Mode (ECM) and the accompanying evolution of fluctuation characteristics. A frequency chirping coherent mode arises as the plasma enters a well-developed H-mode phase. Figure 6 shows evolutionary snapshots of dispersion plots capturing ECM and accompanied recurrence of fluctuations at the H-mode phase in the reference discharge. An ECM begins to nucleate at t =7.15 sec with f~ 60 kHz. The amplitude of ECM strengthens as the transition proceeds. The ECM begins to appear at the highest T_e . Determining the dominant change in plasma parameters that could govern the time trace of ECM is of importance to identify ECM. At t=7.4 sec, the frequency is almost fixed while the density and T_e are still evolving. In spite of the difficulty, however, one may conceive that the relation $\omega_{ECM} \sim f(t)[b+cT_e(t)]^{1/2}$ may potentially reproduce the chirping behavior of ECM. Here, f(t) is a time varying parameter, while b and c are constants. This is just one possible proposition whose validity must be elaborated further.

As the plasma enters a well-developed H-mode state, the frequency of ECM declines, i.e., frequency chirping. As the frequency chirps down, the wavenumber also decreases, keeping the phase velocity of the mode nearly constant during the transition. When the ECM attains a steady state in the H-mode state, distinct types of T_c fluctuations develop as shown in Figs. 6(b)–6(d). One can make a couple of interesting observations. Firstly, the diminished low-frequency modes (both e-and i-modes) begin to reappear as the ECM becomes stronger. These low-frequency fluctuations exhibit no apparent dispersion characteristics. Secondly, one can observe higher (than the ECM)-frequency ion modes with a rather clear indication of a group velocity, as one can see in Fig. 6(d). The sign of the group velocity is negative. This fact implies that the equilibrium E×B velocity is to be excluded as the origin for this $\langle v_g \rangle$ since an E_r -well structure in the H-mode generates positive $\langle v_g \rangle$. Thirdly, the ECM acts like a pivot between the low- and high-frequency fluctuation branches. This observation strongly suggests that the ECM should play a triggering role in both types of fluctuations. Finally, the second harmonics of the ECM appears as the ECM intensifies, as shown in Figs. 6(c) and 6(d). The appearance of the second harmonic mode indicates the existence of a strong nonlinear interaction between the plasma and ECM.

The observations described above demonstrate that the ECM plays a key role in fluctuation evolution during LH transition. Therefore, further investigation of the ECM is necessary to provide a physics-based insight into its role and identity. We first examine the radial variation of the ECM measured by radially aligned ECEI channels, whose results are shown in Fig. 7, displaying spectrograms measured by a set of ECEI channels at different radial positions in the midplane. The measurement range of the horizontal region is 2.11 < R (m) < 2.20. The ECM is observed only at the near-edge region, i.e., when R > 2.20 (m). Because of the extremely high signal-to-noise ratio, we were unable to measure fluctuations beyond R = 2.18 (m), including inside the pedestal. However, we can infer from Fig. 7 that the ECM only resides at the edge and core-pedestal top boundary regions. The radial region where ECM is observed is in contrast to that of QCM in the ECRH-induced EDA H-mode in AUG. Note that the latter is localized near the separatrix [7], while ECM in KSTAR ECH driven H-mode radially extends up to $r/a \sim 0.85$.

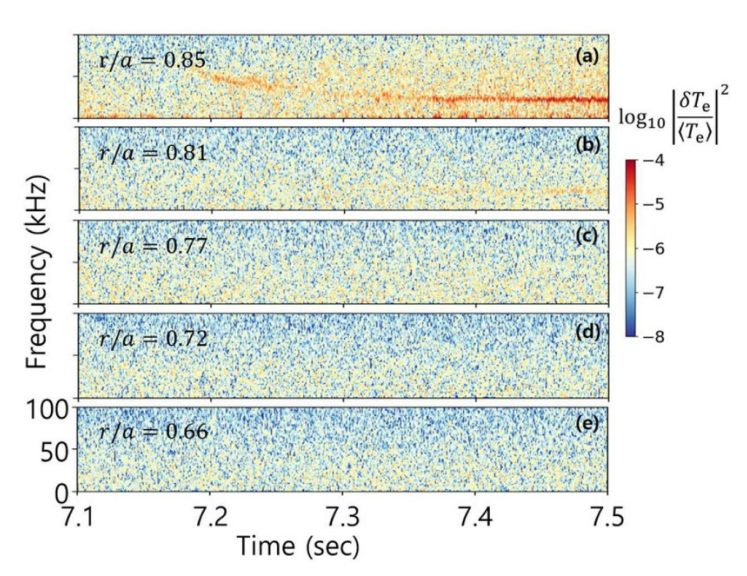


FIG. 7. Radial variation of ECM spectrograms measured by ECEI channels placed at the midplane. Range of the measured horizontal region is 0.66 < r/a<0.85 from the bottom. Beyond r/a=0.85 (a), the ECEI measurement is unreliable due to high signal-to-noise ratio. ECM is shown to reside beyond, at least, r/a>0.81, (b), corresponding to the edge and the core-pedestal boundary regions. [H Jhang et al, Phys. Plasmas, 31, 092501; licensed under a Creative Commons Attribution (CC BY) license]

The emergence of ECM during the ECRHdriven LH transition is consistent with a recent experimental result in AUG where a similar coherent mode is observed during the LH transition [4]. An interesting fact is that a similar phenomenology to QCM at

AUG is also observed in ECM at KSTAR, despite the significant density difference. Note that the stationary ELM-free H-mode in AUG operates at a high L-mode density, while KSTAR LH transition experiments in this paper are carried out near n_{min}. For instance, n_{min} in KSTAR is comparable to the density level of the I-phase at AUG before the fully developed H-mode. In many tokamak experiments, the appearance of a coherent mode has been known to alter edge stability and, as a result, the ELM type, even though its physical mechanism is yet to be

explored. Usually, experimental results show that the ELM type changes from large type I to ELM-free or small ELMs when the coherent (or quasi-coherent) mode persists. For instance, the H-mode plasma in AUG exhibits an ELM-free state in the presence of QCM, even though the power injected is well above the LH transition power threshold [4]. In KSTAR, we compared the ELM types for two H-mode discharges one for ECRH only and the other NBI heated plasma with ~10% higher power level. No coherent mode is observed in the NBI-heated H-mode discharges. We find that the H-mode in the presence of ECM indeed exhibits ELM-free or small ELMs. This fact is in accordance with experimental results reported from other devices in spite of varying mode characteristics. Therefore, the KSTAR ECRH H-mode experiments demonstrate the role of an edge coherent mode in regulating the type-I ELM, suggesting that this should be a universal phenomenon.

5. EDGE LOCALIZED ALFVENIC MODE: A POSSIBLE EDGE COHERENT MODE

A theoretical study of the identity and chirping behavior of the Edge Coherent Mode (ECM) is of great interest for both fundamental and practical reasons. In this section, we explore the edge-localized Alfvén mode as a candidate. The bootstrap current (J_{BS}), driven by a steep edge pressure gradient, modifies the local magnetic shear and thereby influences the Alfvén continuum structure. This, in turn, affects the stability and characteristics of edge Alfvén eigenmodes (AEs). We present a numerical investigation of the impact of the bootstrap current on edge AE properties, employing equilibrium reconstructions and the Kinetic Alfvén Eigenmode Solver (KAES). Our analysis emphasizes the critical role of kinetic damping, impurity content, and pedestal collisionality in shaping AE behavior.

The bootstrap current, computed using neoclassical theory based on observed temperature and density gradients, is incorporated into the CHEASE code through an iterative process. This method calculates a modified, ideal MHD-stable equilibrium that accurately captures the changes in the magnetic shear and q-profile. This modified equilibrium, along with experimental profiles, is then used as input for the Kinetic Alfvén Eigenmode Solver (KAES). KAES estimates Alfvén Eigenmode (AE) damping rates, incorporating key kinetic effects such as FLR corrections and parallel currents. To investigate the full spectrum of potential instabilities, damping rates and mode frequencies are scanned across a range of beta (β) values to observe transitions between different AE types, including the formation of kinetic Toroidal Alfvén Eigenmodes (TAEs). Both low-n (n=1,2) and higher-n modes were studied. Special attention was given to how changes in plasma β , the collisionality parameter (ν) , and the effective charge (Z_{eff}) affect both the equilibrium profiles and the characteristics of the Alfvén continuum.

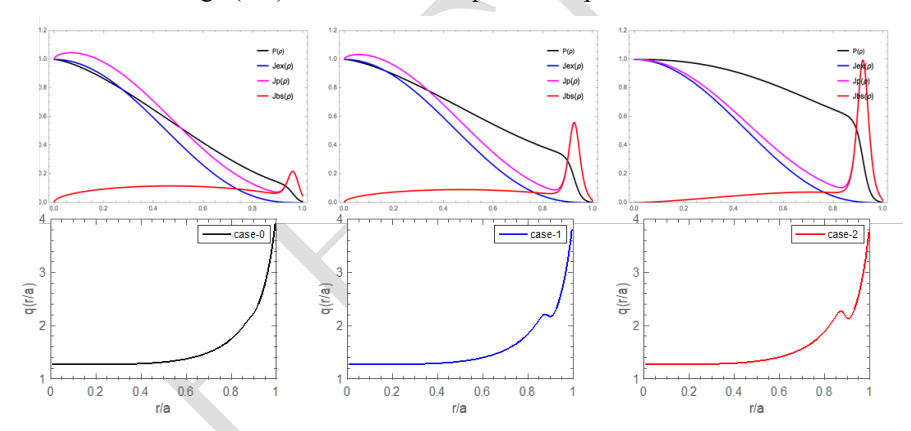


FIG. 7. Effect of pressure gradient on bootstrap current and corresponding q-profile.

Figure 7 illustrates the effect of the bootstrap current on the q-profile modification. The figure presents three cases: Case III, which uses a slightly exaggerated pressure profile to highlight the coupling of neighbouring localized modes, and Cases I and II, which are based on experimental data. For the rest of the paper, we use Case II, as it provides a realistic representation of the experimental profiles. Figure 8 shows the Alfvén continuum (AC), plotted using the KAES code for profile types I, II, and III. The AC is modified by reverse magnetic shear at r/a≈0.88, which leads to the emergence of edge-localized Alfvén eigenmodes (ELAEs) with varying damping characteristics.

Figure 9 shows the Alfvén continuum for the Case II equilibrium. It identifies three distinct types of Edge Localized Alfvén Eigenmodes (ELAEs), with their corresponding radial and poloidal mode structures shown in the right pannel in Fig. 9.

• Type-0 modes have a dominant poloidal mode number m and a frequency nearly identical to that of a Toroidal Alfvén Eigenmode (TAE) gap. These modes are strongly coupled with the (m-1) mode, leading

- to two dominant poloidal components. Their damping characteristics are similar to TAE gap modes; they exist even without kinetic effects and are primarily subjected to radiative damping.
- Type-I and Type-II modes have a finite frequency due to kinetic effects. They are highly localized and each has only one dominant poloidal mode: Type-I has m, while Type-II has (m+1). Both are subject to electron collisional and radiative damping.

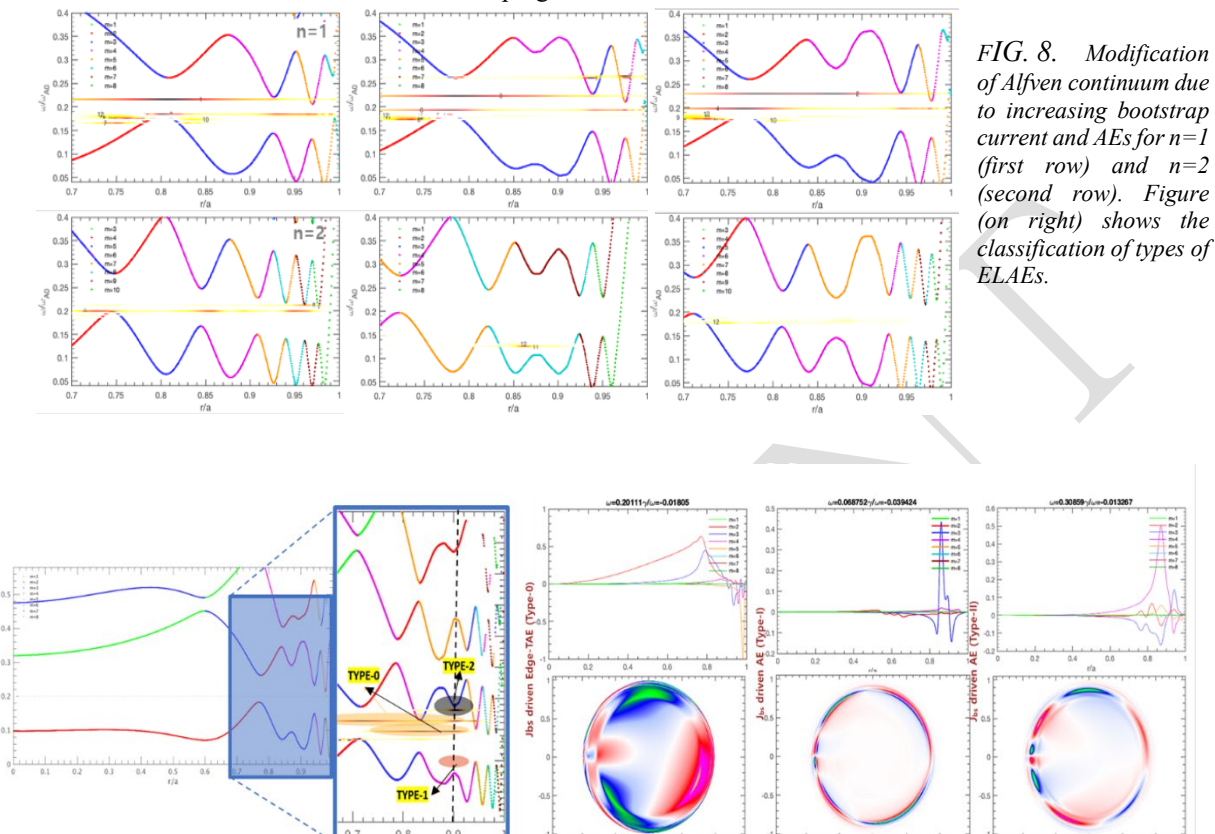
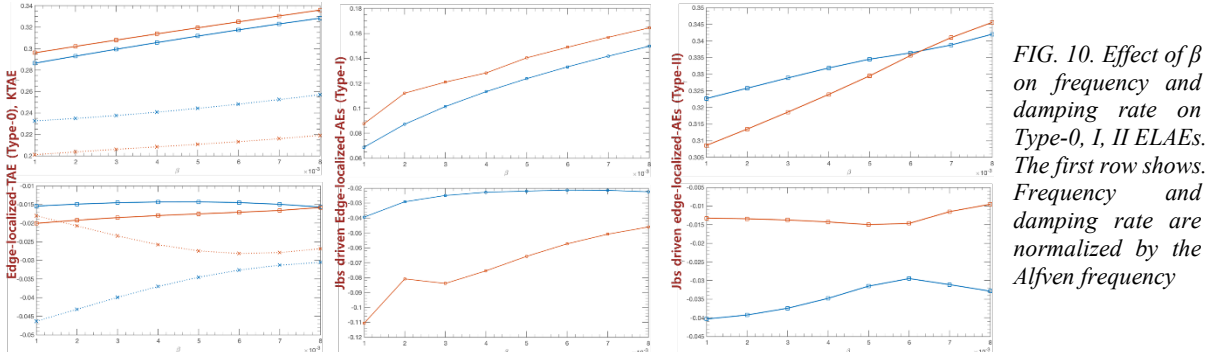


Figure 9 (left) AC and three types of ELAEs, (right) their corresponding radial and mode poloidal structure, and radial location in Alfven continuum.

Figure 10 presents the variation of ELAE frequencies and damping rates with changing plasma beta (β). Due to the presence of kinetic effects, multiple modes exist; two are plotted for each case. The top row of Fig. 4 illustrates how mode frequency (ω) changes with β , while the bottom row shows the corresponding damping rate (γ). The Type-0 (edge TAE-type) ELAEs have a frequency of approximately $\omega \sim \omega_{TAE}$ and exhibit minimal damping. As plasma beta (β) increases, their frequency rises while their damping remains nearly constant. The Type-I ELAEs have a very small frequency, i.e., $\omega \ll \omega_{TAE}$. Their frequency depends on both the magnitude of the bootstrap current and plasma beta. A key characteristic is that their damping decreases as β increases. In our specific case, $\omega/\omega_{TAE} \sim 0.2$ for smaller beta and $\omega/\sim 0.42$ for larger one. The Type-III ELAEs exhibits a frequency band $\omega_{KTAE} > \omega > \omega_{TAE}$. With increasing plasma beta, these modes undergo a transition and convert to Kinetic Toroidal Alfvén Eigenmodes (KTAEs).



It is important to note that both Type II and Type III ELAEs exhibit finite parallel (k_{\parallel}) and perpendicular (k_{\perp}) wavenumbers. This feature places them in the class of Kinetic Alfvén Eigenmodes (KAEs), which are defined by the presence of both parallel and radial components of the perturbed electric field. Furthermore, these modes are highly localized in the radial direction, typically confined to narrow regions near the edge pedestal. This localization property is consistent with the experimental observation presented in Fig. 7.

The mechanism by which this edge coherent mode (or ELAE) prevents ELM collapse is still under investigation. However, a possible scenario linking the evolution of AEs to ELM suppression can be conceived. For a premature or weak pedestal, the pressure gradient is not strong enough to drive a kinetic ballooning mode (KBM). In this case, the AE is not able to transition to a KBM, while coherent AEs can be excited. Then, the EPED model [8] predicts no pedestal collapse. If a stronger pedestal builds, however, the KBM is excited (corresponding to an AE-to-KBM transition), which, in the framework of the EPED model, drives Type-I ELMs. In this circumstance, the coherent mode is expected to disappear. This scenario is likely consistent with the observations in KSTAR presented in this paper. A more detailed analysis is now underway to further elucidate the role of various coherent modes in the pedestal region below the ideal MHD limit.

6. SUMMARY AND CONCLUSIONS

We have conducted an experimental analysis of characteristics of the ECRH-produced LH transition in KSTAR. Particular emphasis is put on the evolution of T_e fluctuations during the confinement regime evolution. A scan of pre-transition density is carried out for a fixed maximum ECRH power available in KSTAR. A comprehensive study of T_e fluctuation evolution has been carried out using ECEI at the core-edge boundary region. When the applied ECRH power increases, a clear dispersion diagram of T_e fluctuations is observed.

During the ECH-induced LH transition, we observe a coherent mode that begins with a high frequency (~60 kHz) and chirps down to ~20 kHz as the transition develops. This observation is in line with that in AUG where a similar coherent mode is found during the high-density ECRH-driven LH transition akin to the EDA H-mode [4]. It is remarkable that the phenomenology is the same at both machines, in spite of the significant disparity in density before LH transition. The coherent mode in KSTAR is located beyond the core-pedestal top boundary region, while the QCM in AUG has been shown to be localized near the separatrix. A possible correlation between ECM and the disappearance of type-I ELMs is shown to occur in our experiments. The potential role of ECM in regulating large ELMs, therefore, is likely to be a universal phenomenon. An interesting observation related to the ECM is that edge turbulence, once reduced during the LH transition phase, revives at a H-mode state. The revival of turbulence lowers the pedestal top pressure, which could be a possible origin of the absence of type-I ELMs after the ECM emerges. As a possible identity for the Edge Coherent Mode (ECM), we explored the excitation of ELAEs by the bootstrap current in the edge pedestal. We propose that the evolution of these edge AEs could be a candidate mechanism for the prevention of ELMs when the coherent mode is present.

ACKNOWLEDGEMENTS

The This work was supported by the R&D Program through the Korea Institute of Fusion Energy (KFE) funded by the Ministry of Science and ICT of the Republic of Korea (Nos. KFE-EN2501-16 and KFE- EN2541-11).

REFERENCES

- [1] GOHIL, P., EVANS T. E., FENSTERMACHER, M. E. ET. AL., Nucl. Fusion 51 (2011) 103020.
- [2] MORET, J.-M., AHMED, S. M., ALBERTI, S., ET. AL., Plasma Phys. Control. Fusion 44 (2002) B85.
- [3] RYTER, F., RATHGEBER, S. K., BARRERA-ORTE, L., ET. AL., Nucl. Fusion 53 (2013) 113003.
- [4] GIL, L. SILVA, C., HAPPEL, T., ET. AL., Nucl. Fusion 60 (2020) 054003.
- [5] RYTER, F., BARRERA-ORTE, L., KURZAN, B., ET. AL., Nucl. Fusion 54 (2014) 183003.
- [6] YAN, Z., MCKEE, G. R., FONCK, R., ET. AL., Phys. Rev. Lett. 112 (2014) 125002.
- [7] KALIS, J., BIRKENMEIER, G., MANZ, P., ET. AL., Nucl. Fusion 64 (2024) 016038.
- [8] SNYDER, P. B., OSBORNE, T. H., BURRELL, K. H., ET AL., Phys. Plasmas 19 (2012) 056115.